Local structural power exponent as an indicator of elastic heterogeneity in glasses

Xuerui Wei [ORCID],[1] Weihua Wang,[2] and Pengfei Guan [ORCID][1,*]

[1]*Beijing Computational Science Research Center, Beijing 100193, China*
[2]*Songshan Lake Materials Laboratory, Dongguan 523808, China*

The origin of the nontrivial power-law relationships between atomic packing density and the related structural properties is considered to be a key puzzle in understanding the nature of glasses. Here, we report the direct link between the medium-range structural evolution and elastic heterogeneity by systematically investigating the packing-density-dependent properties of various glasses based on extensive large-scale molecular dynamics simulations. It is shown that the power exponent of the peaks corresponding to the medium-range orders on the pair correlation function converges to the exponent of the first diffraction peak rather than the Euclidean dimension. This exponent can be regarded as an indicator of heterogeneous mechanical properties. The global power-law relationship results from intrinsic mechanical heterogeneity, with the nontrivial power-law response being a local feature. Our finding provides a different perspective on order in disordered materials and sheds some light on the structural-property relationship in glasses.

I. INTRODUCTION

Metallic glasses (MGs) have attracted massive attention because of their unique properties for potential widespread applications [1–3]. These properties are believed to arise from the nature of MG structure, in which there is no long-range translational order or orientational order, but some degrees of short- and medium-range order [4,5]. Previous studies have identified minority-atom-centered clusters as the short-range order in MGs [6]. So far, several structure models, from the short to medium-range scales, have been proposed to describe the structure of MGs, e.g., random packing of hard-sphere [7], dense cluster packing model [5], packing of quasiequivalent clusters [4], while the understanding of medium-range order (MRO) remains incomplete. Recently, the fractal concept has been introduced to describe the MRO by discovering the well-known noncubic structural power law (SPL) in the reciprocal and real space of MGs as their microscopic structure changes in response to mechanical deformation [8] or composition change [9]. Diffraction experiments [10] for metallic glasses show that there is a general relationship between the mean atomic volume per atom (v_a) or number density (ρ) and the first diffraction peak position (FDP, q_1): $\rho \propto q^{D_q}$ with $D_q \cong 2.5$ deviating from the Euclidean dimension ($D = 3$). However, computational simulation [11] argued that the D_q is in a range (2.5–4.0) for various model MGs and there is no fractal behavior in real space by measuring the mass/density distribution. Moreover, the SPLs with various D_q are also found in different disorder systems, such as alloy liquids [12,13], hard/soft sphere model [14], granular system [15], and exhibit the pressure dependence [16,17], which indicates

that the SPL deviating the Euclidean dimensions of samples is a universal phenomenon in disorder systems.

For crystals, the FDP (q_1) equals $2\pi/d_0$, representing the maximum crystalline interplanar distance (d_0) according to Bragg's law; while amorphous materials are generally believed to be derived from MRO of atomic structure, there is no unified interpretation [18–21]. The q_1 in network-forming materials, e.g., SiO_2 [22], correlates with an intermediate-range structure, such as the connection of local network-forming motifs, reflecting the MRO in real space. However, for MGs, e.g., $Pd_{42.5}Ni_{7.5}Cu_{30}P_{20}$, the FDP ($q_1$) is approximately $2\pi/r_1$, where r_1 is related to the mean nearest-neighbor distance of atoms in real space, corresponding to the structural short-range order (SRO). Thus, how to relate the SPL in reciprocal space to the structure change in real space is the key to understanding the microstructure of atomic glasses, such as MGs. Recent experiment [23] observed the SPL in real space [$\rho \propto r_i^{-D_{r_i}}$, r_i is the ith peak position of the pair correlation function $g(r)$] with D_{r_i} ($i = 1, 2, 3, 4$) approximately equal to D_q (~ 2.5) for the first four peaks of $g(r)$ of Ti-Cu MGs. However, theoretical simulations [11,14] show that the SPL exponent (D_{r_i}) in real space from short range to medium range does not remain constant, but gradually converges to a constant exponent. Thus, though the nontrivial SPLs in disorder materials may arise from nonaffine deformation [11] or ununiform local deformation [14] according to previous studies, the ambiguous link between reciprocal space SPL and real space SPL challenges further understanding of the atomic structure and mechanical response of amorphous materials.

Here we summarize five questions: (1) How does the SPL in real space change from short range to medium range in different glassy systems? (2) Does the SPL in real space quantitively correlate with the SPL in reciprocal space? (3) Does the SPL generally hold in local scales? (4) Which physical properties of static configuration affect the local SPLs? (5)

*pguan@csrc.ac.cn

Can we represent the global SPL by the local SPLs? We try to answer the five questions by systematically analyzing the structure change at different length scales in various glasses under mechanical compression. Quantitative relationships among the reciprocal space SPL, the real space SPL, the local SPLs, and local elastic heterogeneity in glassy materials were established.

II. MATERIALS AND METHODS

A. Simulations of various MGs

We performed molecular dynamics simulation for Ta, Cu, $Cu_{50}Zr_{50}$, and $Zr_{50}Cu_{40}Al_{10}$ systems using LAMMPS [24]. The interaction of atoms is described by corresponding embedded-atom method (EAM) potentials Ta [25], $Cu_{50}Zr_{50}$ [26], and $Zr_{50}Cu_{40}Al_{10}$ [27]. The periodic boundary conditions (PBC) were applied to all simulations. For the consideration of computing resources, we prepared Ta, Cu, and $Cu_{50}Zr_{50}$ large samples containing 1 million atoms by replicating small samples. In comparison, the $Zr_{50}Cu_{40}Al_{10}$ large sample was obtained by quenching the melt containing 1 million atoms directly. Following are the details of the sample preparation.

The small samples containing 8000 atoms in a cubic box were prepared by quenching the equilibrium melt to 300 K temperature with a high cooling rate of 10 K/ps (1 K/ps for $Cu_{50}Zr_{50}$) and relaxed 1 ns at 300 K temperature. Second, the small glassy samples were replicated five times in three dimensions ($5 \times 5 \times 5$) and relaxed 100 ps at 2500 K (1100 K for Cu and 900 K for $Cu_{50}Zr_{50}$). The large samples were relaxed at 1 K temperature for 100 ps to obtain a low-temperature sample. For the $Zr_{50}Cu_{40}Al_{10}$ system, the sample was first equilibrated at 2000 K for 0.5 ns, followed by quenching to 1 K with a cooling rate of 1 K/ps, and further relaxed at 1 K for 0.5 ns. All quenching and relaxation processes were performed in an *NPT* (the number of atoms and the external pressure keeps constant) ensemble with zero pressure by Nose-Hoover [28] thermostat and Parrinello-Rahman [29] barostat. The MD time step is 2 fs. Moreover, we obtained the inherent structures (ISs) of Ta, Cu, $Cu_{50}Zr_{50}$, and $Zr_{50}Cu_{40}Al_{10}$ glassy samples by performing energy minimization. These samples without thermal effect will be used to analyze the evolution of atomic structure under compressive deformation and study the SPL.

We performed athermal quasistatic (AQS) compression on Ta, Cu, $Cu_{50}Zr_{50}$, and $Zr_{50}Cu_{40}Al_{10}$ glassy samples in three dimensions. After each strain step, $\Delta\delta = 0.001\%$, the system's potential energy was minimized to local minima by a conjugate gradient algorithm. The maximum linear strain is -2%, where "$-$" denotes compressive deformation. During the AQS compression, the five representative atomic configurations corresponding to 0%, -0.5%, -1%, -1.5%, and -2% strain states were collected for analysis of the evolution of structure.

B. Structure factor $S(q)$

There are two equations to calculate the structure factor:

$$S(\vec{q}) = \frac{1}{N} \sum_{j=1}^{N} \sum_{l=1}^{N} \langle \exp[-i\vec{q} \cdot (\vec{r}_j - \vec{r}_l)] \rangle, \quad (1)$$

$$S(q) = 1 + \rho \int_0^\infty (g(r) - 1) \frac{\sin(qr)}{qr} 4\pi r^2 dr. \quad (2)$$

Equation (1) indicates that the structure factor can be calculated directly from the position of all atoms (N is the number of atoms), where $\vec{r}_j$ represents the position of the jth atom, $j = 1, \ldots, N$, and $\langle \cdots \rangle$ denotes the ensemble average. Equation (2) shows that the structure factor $S(q)$ can be obtained by calculating the Fourier transform of pair correlation function $g(r)$. We calculated the structure factor of Ta glass by two methods. The shape of $S(q)$ obtained by the two equations has no difference approximately, while Eq. (2) produced a smoother peak that is useful for determining the peak position precisely. Therefore, we use Eq. (2) to calculate the $S(q)$.

C. Microscopic mechanical properties

The procedure to calculate the atomic bulk modulus (ABM) is similar to the local bulk modulus described by Mizuno *et al.* [30]. In principle, the ABM includes three parts, $K_i = K_i^B + K_i^N + K_i^k$, where K_i is the ABM and K_i^B, K_i^N, and K_i^k represent the Born term, nonaffine term, and kinetic energy term, respectively. The K_i^k equals zero at zero temperature and K_i^N shows a tiny contribution to the ABM. Therefore, $K_i \simeq K_i^B$ at zero temperature, and we can use the affine deformation approach to calculate the ABM,

$$K_i = \frac{p_{i,1} - p_{i,0}}{-3\varepsilon}, \quad (3)$$

where ε is the linear strain of isotropic affine deformation; the trace of the stress tensor (σ_i) is atomic level pressure $p_i = -(\sigma_i^{xx} + \sigma_i^{yy} + \sigma_i^{zz})/3$. σ_i^{xx} is the component of the stress tensor (σ_i) in the xx direction. $p_{i,0}$ and $p_{i,1}$ are the atomic level pressure of the ith atom at the initial and small strain states. In this work, we use 0.1% affine deformation to calculate the ABM for these MGs.

III. RESULTS

A. SPLs in real space from SR to MR

We prepared three kinds of model MGs, i.e., monatomic (Ta [25], Cu), binary ($Cu_{50}Zr_{50}$ [26]), and ternary ($Zr_{50}Cu_{40}Al_{10}$ [27]) MGs based on the embedded-atom method (EAM) potentials. The related data of $Ti_{62}Cu_{38}$ bulk metallic glasses (experiment) [23], the two-dimensional (2D) hard/hard sphere (2DHH) models, 2D Week-Chandler-Andersen (2DWCA) models, and 2D hard/soft sphere (2DSH) models [14] in previous works are also included for analyses.

The evolution of calculated $g(r)$ under isostatic compression up to 2% linear strain is shown in Fig. 1(a) and in Figs. S1(a)–S1(c) of the Supplemental Material [31]. The peak positions (r_i) of $g(r)$ are shrinking with the increase of strain, indicating the decrease in average interatomic distance. The SPL exponents (D_{r_i}) of different peaks can be extracted by fitting the relation between the density (ρ) and the related peak positions of $g(r)$, r_i, as shown in Fig. 1(b) and Fig. S2 [31]. It is clear that different peaks behave as distinct SPLs. Figure 1(c) shows the D_{r_i} ($i = 1, 2, 3, 4, 5, 6, 7$) values extracted from the model MG samples investigated by us, and other systems studied in previous works, including neutron diffraction
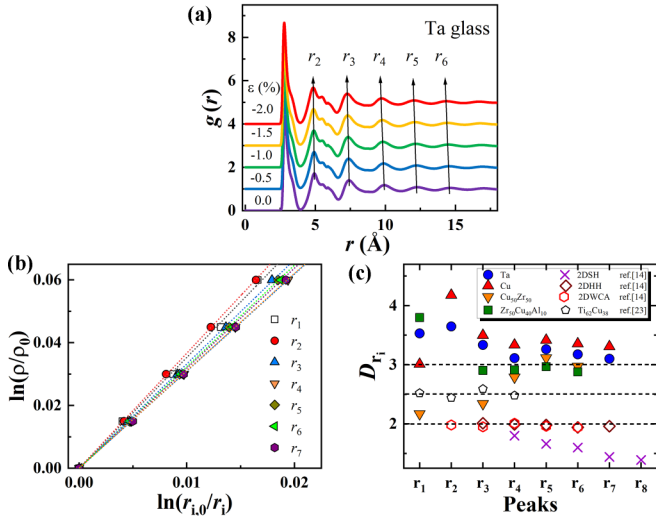
FIG. 1. The structural power laws (SPLs) of real space. (a) Evolution of pair correlation function $g(r)$ of Ta glass at representative strain states. (b) Scaling relationship between $\ln(\frac{\rho}{\rho_0})$ and $\ln(\frac{r_{i,0}}{r_i})$ for Ta glass, the SPLs in real space, where ρ is density, $r_1, r_2, \ldots, r_7$ correspond to the peak positions of $g(r)$. The subscript "0" indicates the initial state with zero strain. (c) SPLs of $g(r)$ from r_1 to r_8 for both metallic glasses and two-dimensional model systems. The D_{r_i} exhibits a plateau at the medium range. We choose the D_{r_i} of the maximum peak as a representative point of the SPL and named D_r. The data of 2DSH, 2DHH, and 2DWCA systems comes from Zhang *et al.* [14], and $Ti_{62}Cu_{38}$ from Li *et al.* [23]. The D_{r_2} of $Cu_{50}Zr_{50}$ and $Zu_{50}Cu_{40}Al_{10}$ are not shown in here; since the position of second peak of $g(r)$ is nearly constant, in contrast the shape clearly presents change under deformation.
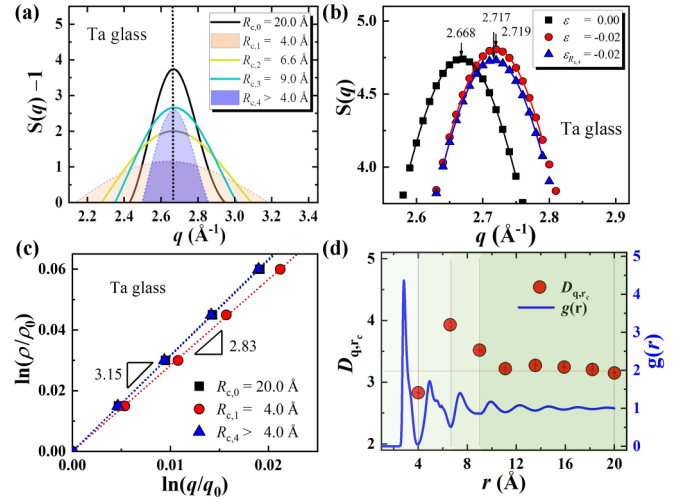

FIG. 2. The SPL of reciprocal space and the shift of the FDP. (a) FDP of reduced structure factor $S(q) - 1$ at five kinds of cutoff distances. The solid black line is the total structure factor, while the peaks with green and blue color represent the FDP of short- ($R_{c,1} = 4$ Å) and medium-range structure ($R_{c,4} > 4$ Å), respectively. (b) Shift of FDP at 0% and −2% strain states (the "−" represents compressive strain). The blue triangle curve is the FDP induced by the evolution of medium-range structure ($R_{c,4}$) under compressive deformation. (c) SPL of Ta metallic glass. The black square line is the sample's SPL, while the red circle and blue triangle lines indicate the SPLs of short- and medium-range structures, respectively. The q and ρ are the peak position of FDP and the density of the sample, respectively. (d) Evolution of SPLs, D_{q,r_c}, within the increasing cutoff distance (r_c). The solid blue line is the pair correlation function $g(r)$ of Ta metallic glass, as a comparison with the D_{q,r_c}. The red horizontal line denotes the plateau of D_{q,r_c}, at a medium-range scale.

experiment [23] and numerical simulations of 2D models [14]. With the increase of r_i, the D_{r_i} value of each system converges to a plateau. However, the convergence value of D_{r_i} (defined as D_r) is different for each system: D_r of systems $Cu_{50}Zr_{50}$ and $Zr_{50}Cu_{40}Al_{10}$ is ~ 3, D_r of systems 2DHH and 2DWCA is ~ 2, and D_r of systems Ta, Cu, $Ti_{62}Cu_{38}$, and 2DSH is 3.10, 3.31, 2.48, and 1.39, respectively. It reveals that the exponents of the power laws from the medium-range real-space structures do not always result in the trivial $D_r = d = 3$ or 2 [11,14], which is the Euclidean dimension of system. The various SPLs in real space from short range to medium range reflect the distinct mechanical responses of disorder structure at different length scales.

B. From real space to reciprocal space

Taking the advantage of MD simulation and the Fourier transform, we can directly calculate the pair correlation function $g(r)$ and establish the quantitative link between the real-space atomic structure and the reciprocal-space structural factor $S(q)$ that can be directly measured from diffraction experiment. To detect the contributions of real-space structure at short and medium ranges to the SPL in reciprocal space, we select different integral ranges of r in the Fourier transform and obtain the corresponding $S(q)$. The selected integral ranges are $R_{c,1}$ ([0, 4.0 Å]), $R_{c,2}$ ([0, 6.6 Å]) and $R_{c,3}$ ([0, 9.0 Å]), which respectively correspond to the real-space

length scale up to the first three minima of $g(r)$, and $R_{c,4}$ ([4.0, 20.0 Å]) which excludes the contribution of short-range structure information. The corresponding $S(q)$ are denoted as $S_{R_{c,1}}(q)$, $S_{R_{c,2}}(q)$, $S_{R_{c,3}}(q)$, and $S_{R_{c,4}}(q)$, respectively. The $S(q)$ integrated from the range $R_{c,0}$ ([0, 20.0 Å]) is regarded as the total structural factor $S_T(q)$. Figure 2(a) shows the FDP of the reduced structure factor $[S(q) - 1]$ integrated from five regions. As the upper bound of the integral range (r_c) increases from 4.0 to 20.0 Å, the intensity of the FDP is enhanced monotonously. However, the peak position of the FDP is almost the same; the FDP of $S_{R_{c,1}}(q)$ and $S_{R_{c,4}}(q)$ are equal to 2.64 and 2.67 Å^{-1}, respectively. It indicates the same hidden order in the real space structure of MGs from short range and medium range.

The previous studies suggest that the FDP corresponds to medium-range atomic correlation in real space [32,33], and the other peaks at high-q represent SRO [9,34]. Recently, Salmon *et al.* [22] found that the MGs and amorphous network materials all exhibit diffraction peak at $q \approx 2\pi/r_1$, where r_1 is the mean interatomic distance and approximately the first peak position of $g(r)$. However, this peak is the FDP of MGs, but the second or third diffraction peak of amorphous network materials. This means that the amorphous network materials can exhibit medium-range order in the range of $q < 2\pi/r_1$, whereas the position of FDP ($q_1 \approx 2\pi/r_1$) of strain-free MGs

seems to be determined by the nearest-neighbor atomic distance (short range).

The response of FDPs, corresponding to real-space structure information in different length scales, to a compressive strain of 2% is shown in Fig. 2(b). The right shifts of FDPs indicate the decrease of interatomic distance under compressive strain. The blue triangle lines represent the combinational $S(q)$ based on the strained $S_{R_{c,4}}(q)$ and the unstrained $S_{R_{c,1}}(q)$. In other words, if the integrating range is set as $R_{c,4}$ ([4.0, 20.0 Å]) to exclude the contribution of the real-space short-range structure information to $S(q)$, we can still get the same response as $S_T(q)$. The same peak position indicates that the shift of FDP of $S_T(q)$ is dominated by the structural evolution beyond the short-range length scale in real space. The SPLs of related $S(q)$ are presented in Fig. 2(c), and the extracted $D_{q,R_{c,1}}$ is ~ 2.80, which is different from $D_{q,T} \sim 3.15$ and $D_{q,R_{c,4}} \sim 3.16$. Note that the average value of the local volumetric strain is independent of the cutoff distance (shown in Fig. S3 [31]), so we can use the macroscopic volumetric strain to fit SPLs on different length scales, as shown in Fig. 2(c).

Figure 2(d) exhibits the D_{q,r_c} of different $S_{r_c}(q)$ obtained by integrating $g(r)$ with different r_c. The D_{q,r_c} values are increased from ~ 2.83 to ~ 3.93 as the r_c increased from 4.0 Å (first shell) to 6.6 Å (first two shells). Therefore, the first and second shells of $g(r)$ exhibit different mechanical responses under macroscopic deformation. It is consistent with the previous x-ray diffraction experiment by Poulsen *et al.* [35], which observed the difference of mechanical response between short- and medium-range structures in MGs by measuring the shift of peak positions of $g(r)$ and FDP under external loading. The D_{q,r_c} rapidly converges to the value of $\sim D_q$ with the increase of r_c, indicating that the evolution of medium-range structure in real space dominates the shift of FDP in reciprocal space. The results show that though the position of FDP (q_1) of stress-free samples is related to the nearest-neighbor atomic distance (r_1), the shift of FDP completely reflects the response of structure in medium-range scale to the external macroscopic strain field. It provides direct evidence that the shift of FDP of total $S(q)$ is mainly contributed by the medium-range structure in real space and implies an intrinsic link between the D_q in reciprocal space and the D_r in real space.

C. Correlation between D_q and D_r

Figure 3(a) shows the evolution of total $S(q)$ of large-scale Ta glassy samples under various isotropic compressive strains. The shifting of FDPs of other systems can be observed in Figs S1(d)–S1(f), and the related peak position can be collected to calculate the D_q. The SPLs for various MG samples are exhibited in Fig. 3(b), and distinct D_q can be extracted, which is consistent with the previous simulation works [11]. A quantitative relation between D_r in real space and D_q in reciprocal space for all systems listed in Fig. 1(c) can be established in Fig. 3(c). Here, the D_r is equal to D_q approximately, independent of the systems and their Euclidean dimensions. Previous theoretical simulations [11,14] show that the SPL exponent (D_{r_i}) in real space from short range to medium range gradually converges to a constant exponent. Here, we provide the direct
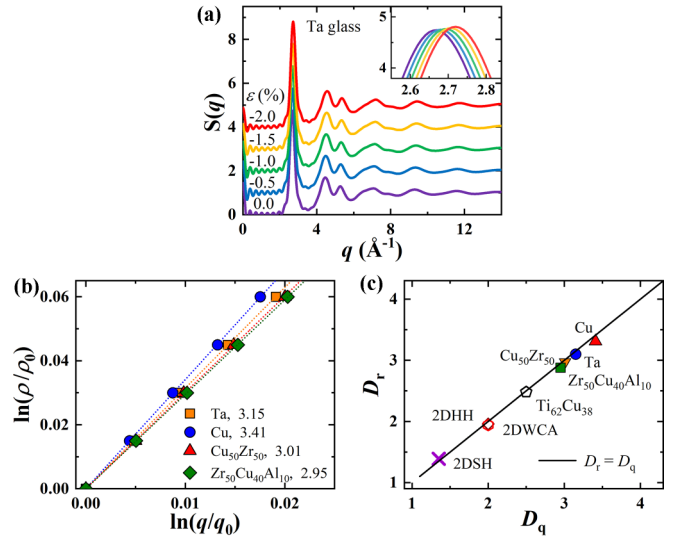

FIG. 3. The correlation of structural power laws in both real space and reciprocal space. (a) Evolution of structure factor $S(q)$ of Ta glass at representative strain states. The inset shows the shift of FDP under compression, where the blue and red lines represent the 0% and -2.0% strain states, respectively. (b) Scaling relationship between $\ln(\frac{q}{q_0})$ and $\ln(\frac{\rho}{\rho_0})$ for Ta, Cu, $Cu_{50}Zr_{50}$, and $Zr_{50}Cu_{40}Al_{10}$ systems, the SPLs in reciprocal space, where ρ and q denote the density of the sample and the FDP. (c) SPL (D_q) of reciprocal space equals the medium-range SPL of real space (D_r) for various systems.

evidence that the SPL in reciprocal space quantitively correlates with the SPL in real space at the medium-range length scales and conclude that the constant exponent in real space is the SPL exponent (D_q) in reciprocal space. It gives us some hints that we may understand the SPL in reciprocal space by systematically investigating the mechanical heterogeneity of amorphous solids in real space.

D. Local SPLs versus local bulk modulus

The inhomogeneous local elastic properties have been studied in experiments [36,37] and atomistic simulations [30,38–40] for amorphous systems. During external loading, the regions with different local elastic properties, such as local bulk modulus and local shear modulus, could have different mechanical responses. Therefore, we proposed that the local SPL [$\rho \propto (q, R_j)^{D_{q,R_j}}$] from the FDP of the local structure factor [$S(q)_{R_j}$] could correlate with the ABM. The q, R_j is the peak position of FDP of local structure factor [$S(q)_{R_j}$] of the R_j region that is selected based on atomic properties, such as the ABM (see the derivation of the local structure factor in the Appendix).

Figure 4(a) shows the spatial map of the ABM of the Ta glass. It is inhomogeneous in real space. The red region exhibits a larger ABM, while the blue region exhibits a smaller ABM. We use black contour lines to circle the largest ABM region, named the R_1 region, and the smallest ABM region, named the R_2 region. Each region contains 10% of the atoms in the system. Figure 4(b) shows the probability distribution function of the ABM and the R_1 and R_2 regions in Ta glass. It is distinct that the two regions are separated and represent the hard region and soft region. The local structure factor
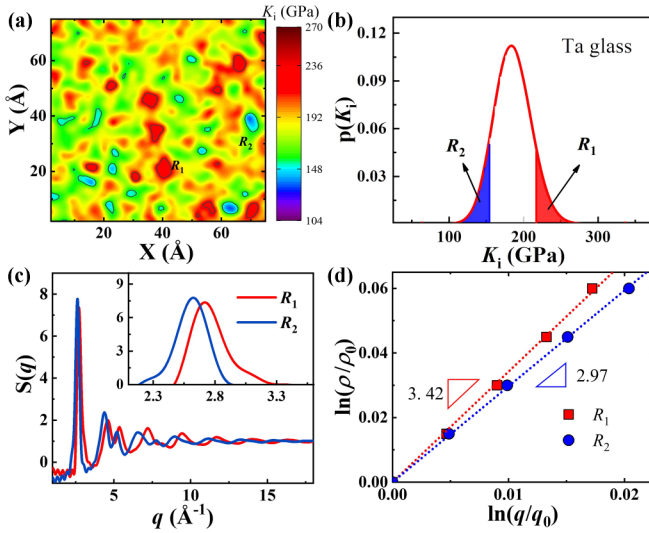
FIG. 4. The spatial maps of the ABM and the local structure factor. (a) Spatial map of ABM of Ta metallic glass. The solid black curves represent the contour line that circles the R_1 region with the largest ABM (red color) and the R_2 region with the smallest ABM (blue color); each region contains 10% atoms. (b) Probability distribution function of ABM in Ta glass and the representative R_1 and R_2 regions. (c) Local structure factor of the R_1 and R_2 regions. The inset shows the enlargement of FDP. (d) Scaling relation between $\ln(\rho/\rho_0)$ and $\ln(q/q_0)$, where ρ is the density and q denotes the FDP of the local structure factor for a region, such as the R_1 or R_2 region. The subscript "0" indicates the initial state.

$[S(q)_{R_j}]$ is calculated by Fourier transformation of the local pair correlation function $[g(r)_{R_j}]$. As shown in Fig. 4(c), the local structure factor of the two representative regions exhibits different FDP, and the FDP shifts to smaller q from the R_1 to the R_2 region, which indicates the two regions possess the densely atomic packing and loosely atomic packing, respectively. As shown in Fig. 4(d), the exponent of the local SPL of the R_1 and R_2 regions are equal to 3.42 and 2.97, respectively. This phenomenon shows they possess different mechanical responses at medium-range scales under hydrostatic compressive deformation.

Figure 5(a) systematically shows the relation between the local SPLs (D_{q,R_j}) and the average value of ABM of R_j regions (K_{R_j}) for Ta, Cu, $Cu_{50}Zr_{50}$, and $Zr_{50}Cu_{40}Al_{10}$ MGs. The D_{q,R_j} decrease with the K_{R_j}, nearly linear relation, which implies that the exponents of local SPLs (D_{q,R_j}) could be dominated by the K_{R_j} of the R_j region. At the same time, the total SPL (D_q) could come from the superposition of local SPLs of regions with different K_{R_j}. To uncover the relation between the local SPL and the total SPL of reciprocal space, we scaled the D_{q,R_j} values and K_{R_j} by the D_q value and the weighted average value of the ABM, $\bar{K}$, of samples, respectively, where $\bar{K} = 1/\sum_{i=1}^{n} \frac{v_{i,0}}{V_0 \cdot K_i}$ derived from the previous work about SPLs [40], and V are the atomic volume of the ith atom and $v_{i,0}$ and V are the atomic volume of the ith atom and the total volume of sample at free strain state, respectively. As shown in Fig. 5(b), the scattered points of Ta and Cu glass were collapsed to a master line passed (1.0, 1.0). A similar result also was observed in $Cu_{50}Zr_{50}$ and $Zr_{50}Cu_{40}Al_{10}$ MGs. In other words, $D_{q,R_j}/D_q \propto K_{R_j}/\bar{K}$, it indicates that the
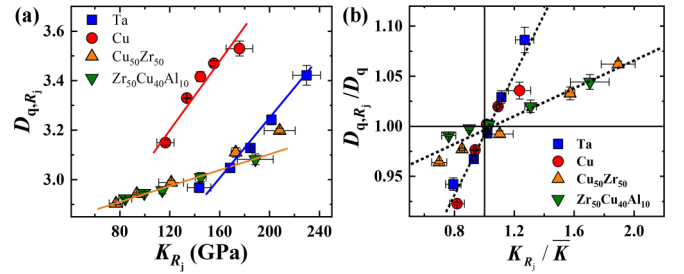

FIG. 5. The correlation between the local SPLs and atomic bulk modulus (ABM). (a) ABM of selected regions and the corresponding local SPLs in Ta, Cu, $Cu_{50}Zr_{50}$, and $Zr_{50}Cu_{40}Al_{10}$ MGs. The horizontal and vertical error bars come from the standard derivation of ABM of R_j region and the fitting error of local SPLs, respectively. (b) Linear relation between the reduced local SPL $(D_{q,R_j}/D_q)$ and the reduced ABM $(K_{R_j}/\bar{K})$. The dashed lines show approximately the slopes.

difference in the ABM between the local region and the weighted average value of the ABM of the sample induces the diverse D_{q,R_j} values that are deviated from the D_q value of the sample. For instance, the R_1, R_2 regions with the largest and smallest ABM exhibit the local SPLs of 3.42 and 2.97, respectively, which deviated from 3.15, the SPL of Ta glass. If the ABM equals the $\bar{K}$, the local SPL is equal to the sample's SPL for various systems.

Moreover, we noted that the monatomic metallic glass exhibits a larger slope than multicomponent MGs in Fig. 5(b), indicating the clearly different medium-range mechanical responses. For instance, the 30% deviation of the ABM between the regions and the sample results in about 8% and 2% differences in mechanical response for monatomic and multicomponent MGs, respectively. This phenomenon implies monatomic MGs exhibit a stronger correlation at medium-range length scales than multicomponent MGs. If the correlation disappears, the medium-range mechanical response will be homogeneous in space, and the local SPL will decorrelate with the ABM of regions; hence the slope will be zero.
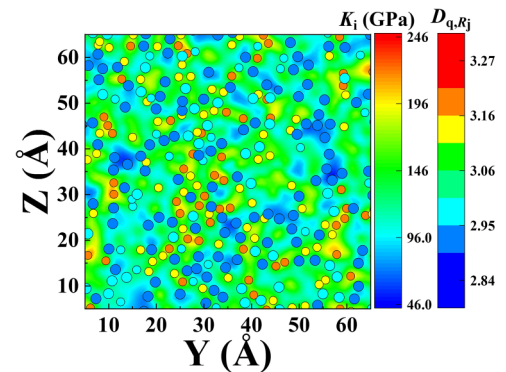

FIG. 6. The spatial distribution of ABM and the local SPLs. The figure shows the spatial distribution of ABM and the local SPLs (D_{q,R_j}) of atoms in the five representative regions in a slice of $Cu_{50}Zr_{50}$ MGs. The large and small atoms indicate the Zr and Cu atoms, respectively. The color background represents the distribution of ABM, while the color of atoms represents the local SPLs.

Figure 6 shows the spatial distribution of ABM in $Cu_{50}Zr_{50}$ MGs. The MG exhibits heterogeneous elasticity and contains the hard (red color) region, soft (blue color) region, and relatively moderate region (green color). This phenomenon relates to structural heterogeneity, such as densely and loosely packed regions. The larger (smaller) circles represent the Zr (Cu) atoms. The color of atoms shows the local SPLs of the representative five regions, where the pattern is very similar to the spatial distribution of the ABM. The hard and soft regions exhibit larger and smaller local SPLs, respectively. Meanwhile, the local SPL of the moderate region is equal to the SPL of the sample. Therefore, we propose that the local SPLs can be used to identify MGs' hard and soft regions as an indicator of mechanical heterogeneity. The traditional methods to measure mechanical heterogeneity are atomic force microscopy [41] or static force spectroscopy [42]. Here, we proposed that diffraction methods by measuring the shift of FDP of local structure factor under macroscopic deformation can be used to characterize the nanoscale mechanical heterogeneity of MGs.

IV. DISCUSSION

In this work, by extensive MD simulations, we found that the SPL of real space exhibits larger fluctuation at short range and shows a plateau region at medium range for various MGs. Moreover, the SPL of reciprocal space equals the SPL of real space at medium-range length scales. It means the evolution of medium-range structure dominates the shift of the FDP of structure factor in MGs, even though the FDP contains both short- and medium-range structure information [Fig. 2(b)]. This finding is consistent with the general knowledge that the FDP reflects the medium-range atomic correlation in an amorphous system [9,19,43]. The critical difference is that with MGs as an atomic packing system the peak position of FDP does not represent the medium-range structure directly but the short-range periodicity for both short- and medium-range structures, whereas the shift of the FDP is dominated by the evolution of medium-range structure, as shown in Figs. 2(b) and 2(c). Consequently, the peak position of the FDP approximately follows Ehrenfest's relation ($q \cong 2\pi k/r$), k is a coefficient, and the shift of FDP represents medium-range structure information. Therefore, the SPL of reciprocal space represents the mechanical responses of the medium-range structure under macroscopic deformation and should not be interpreted as a fractal dimension.

The correlation between the local SPL of reciprocal space and the ABM has been studied in this work. We found that the region with a larger (smaller) ABM presents larger (smaller) values in Ta, Cu, $Cu_{50}Zr_{50}$, and $Zr_{50}Cu_{40}Al_{10}$ MGs. Furthermore, we found $D_{q,R_j}/D_q \propto K_{R_j}/\bar{K}$, which indicates that the local mechanical heterogeneity found in experiments [41,42], and computer simulations [39] play an essential role in the local SPLs of MGs. If the ABM of a given region is larger (smaller) than the average bulk modulus, the corresponding local SPL is larger (smaller) than the SPL of a sample. If the ABM equals the average bulk modulus, the local SPL equals the SPL of a sample. In other words, the local SPL (D_{q,R_j}) will be a parameter to represent the mechanical heterogeneity
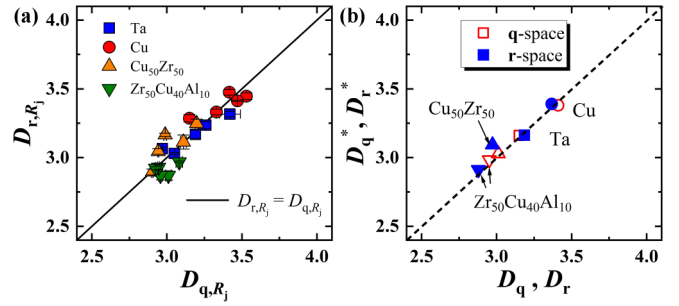

FIG. 7. The correlation between local SPLs and total SPLs in both real and reciprocal spaces. (a) Local SPL in reciprocal space (D_{q,R_j}) is equal to the corresponding local SPL in real space at a medium-range length scale (D_{r,R_j}) approximately. The five points with the same shape represent the same system. (b) Weighted sum of local SPLs is equal to the total SPL in both real space and reciprocal space, $D_q^* \approx \sum_{j=1}^{n} \frac{N_{R_j}}{N} D_{q,R_j}$ and $D_r^* \approx \sum_{j=1}^{n} \frac{N_{R_j}}{N} D_{r,R_j}$, where N_{R_j} denotes the number of atoms in the R_j region, N is the total number of atoms, and n indicates the total number of regions. To distinguish the measured SPLs D_q and D_r, the calculated SPLs are denoted using the D_q^* and D_r^*.

by measuring the shift of the FDP of a local region under macroscopic deformation.

State-of-art experiments will verify the above findings. For example, previous studies have found the local mechanical heterogeneity [42] and structural heterogeneity [44] in MGs by static force spectroscopy and angstrom-beam electron diffraction, respectively. Combining the two methods, one may observe the mechanical responses of nanoscale regions with structural and mechanical heterogeneity in MGs and answer how these local regions respond to external loadings, such as hydrostatic compression. The exponents of the local SPL could be a parameter to link the structural heterogeneity and mechanical heterogeneity at the local level in MGs.

The local SPL of real space ($\rho \propto (r_i, R_j)^{-D_{r_i,R_j}}$) was investigated systematically for Ta, Cu, $Cu_{50}Zr_{50}$, and $Zr_{50}Cu_{40}Al_{10}$ MGs. The ratio of $D_{r_i,R_j}/D_{q,R_j}$ converges to 1 at the medium-range length scale for regions with different ABM (shown in Fig. S4 [31]). It indicates that the local SPL of real space at a medium-range length scale is equal to the local SPL of reciprocal space, like the total SPL in Fig. 3(c), and this phenomenon is independent of the ABM. If we name the local SPL (D_{r_i,R_j}) of a peak at maximum r is D_{r,R_j} as a representation of medium-range local SPL, the D_{r,R_j} will be approximately equal to D_{q,R_j} of the corresponding region, as shown in Fig. 7(a). The D_{q,R_j} is equivalent to the D_{r,R_j} and represents the mechanical response of medium-range structures at the local level. Moreover, we demonstrate that the weighted sum of local SPLs is equal to the total SPL in both real space and reciprocal space, $D_q^* \approx \sum_{j=1}^{n} \frac{N_{R_j}}{N} D_{q,R_j}$, and $D_r^* \approx \sum_{j=1}^{n} \frac{N_{R_j}}{N} D_{r,R_j}$, where n is the number of regions, N denotes the total number of atoms and N_{R_j} indicates the number of atoms in the R_j region (see details of the derivation in the Appendix). Note that the superscript $*$ of D_r and D_q indicates that it is a calculated value. Figure 7(b) verified this demonstration between local SPLs and the total SPLs. In other words, we reproduced the total SPL from the

local SPLs. Thus, we propose that the SPL of both real and reciprocal space originate from the superposition of regions with different ABM. These regions exhibit inhomogeneous mechanical responses under macroscopic deformation and present various local SPLs. The above correlation between the total SPL, local SPL, and ABM suggests a potential relationship between the bulk modulus and the SPL via particle interaction, which may be further studied at particle level in systems with analytic interaction potentials (e.g., Lennard-Jones potential functions).

Furthermore, the experimental measurement of the elastic constants in MGs by diffraction methods presents a systematic difference compared with traditional methods, while the reason remains unclear [3]. According to our findings, we propose that the well-known relation $\varepsilon = \frac{d_1 - d_0}{d_0} = \frac{q_0 - q_1}{q_1}$ to measure strain (ε) in crystals is not followed strictly in MGs due to the mechanical heterogeneity, where d the average interatomic distance, and q the peak position of FDP. The deformed state and initial state are marked by subscripts "1" and "0," respectively. Thus, MGs exhibit nontrivial SPLs under compression deformation. The local and macroscopic strain under external loading may be underestimated or overestimated by measuring the shift of FDP and using the above well-known relation, producing inaccurate elastic constants. Fortunately, this kind of error can be modified according to the exponent of the SPL for a specific system, which is worth studying in the future. The research on the SPL could enhance the experimental technique to measure the elastic constants of MGs by diffraction methods.

V. CONCLUSIONS

In summary, the SPL of both reciprocal and real space in MGs has been systematically studied using MD simulations. The five questions about SPL posed in the Introduction section can be answered directly.

How does the SPL in real space change from short range to medium range in different glassy systems? By analyzing the large data, including MGs and hard/soft sphere model, we found that from the short-range to medium-range length scales, the SPL of the real space exhibits fluctuating character and eventually exhibits a plateau value at the medium range. It means the mechanical response of MGs depends on the length scales such as short range or medium range. Moreover, unlike intuition, the SPL at medium-range scales is not necessarily equal to the Euclidean dimension of the system.

Does the SPL in real space quantitively correlate with the SPL in reciprocal space? The answer is *yes*. The SPL of medium-range scales is equal to the SPL of reciprocal space, as shown in Fig. 3(c). This phenomenon stems from the fact that even though the peak position of the FDP of MGs or disordered packing systems corresponds to short range in real space ($q \approx 2\pi/r$), the shift of the FDP is determined by the evolution of the medium-range structure. Therefore, the SPL of reciprocal space represents the mechanical response of the medium-range structure. It is further verified by investigating structure evolution at different length scales.

Does the SPL generally hold in local scales? We measured the shifting of peak positions of the local structure factor and local pair correlation function of regions and obtained the

corresponding local SPLs. The ratio of local SPLs over the SPL of the sample is proportional to the ratio of the ABM over average bulk modulus among Ta, Cu, $Cu_{50}Zr_{50}$, and $Zr_{50}Cu_{40}Al_{10}$ MGs.

Which physical properties of static configuration affect the local SPLs? The above proportional relation suggests that the local SPL is dominated by the ABM that depends on the specific chemical elements of atoms and their local packing density, such as densely or loosely packed regions. Thus, we propose that the local SPL can be an indicator of the mechanical heterogeneity of MGs.

Can we represent the global SPL by the local SPLs? We have demonstrated that the total SPL of the sample comes from the weighted sum of the local SPLs, as shown in Fig. 7(b).

Our study uncovered the microscopic mechanism of the SPL from both real and reciprocal space, the local and global levels, and revealed the linear relation between local SPLs and the ABM. The local SPLs can be an indicator of the local mechanical heterogeneity of MGs. This work will deepen the understanding of the amorphous structure of the MG and its mechanical response under compressive deformation and give hints to the structure-properties relationship of MGs.

APPENDIX

1. Derivations of the local pair correlation function and local structure factor

It is well known that for amorphous systems, the pair correlation function $g(r)$ has the following form [45], representing the conditional probability of finding an atom at a position far away from a given atom r distance:

$$g(r) = \frac{1}{4\pi r^2} \frac{1}{N\rho} \sum_i \sum_{k \neq i} \langle \delta(r - |\vec{r}_k - \vec{r}_i|) \rangle, \quad (A1)$$

where ρ is the number density of atoms, N is the total number of atoms, and $\vec{r}_i$ and $\vec{r}_k$ denotes the position of the ith atom and kth atom, respectively. $\delta(\ldots)$ is the delta function and $\langle \ldots \rangle$ indicates the ensemble average. If the atoms are classified into n regions according to the atomic-level properties, the $g(r)$ can be rewritten as

$$g(r) = \frac{1}{4\pi r^2} \frac{1}{N\rho} \sum_{j=1}^{n} \sum_{i \in R_j} \sum_{k \neq i} \langle \delta(r - |\vec{r}_k - \vec{r}_i|) \rangle, \quad (A2)$$

$$g(r) = \sum_{j=1}^{n} \frac{N_{R_j}}{N} \left(\frac{1}{4\pi r^2} \frac{1}{N_{R_j}\rho} \sum_{i \in R_j} \sum_{k \neq i} \langle \delta(r - |\vec{r}_k - \vec{r}_i|) \rangle \right), \quad (A3)$$

where N_{R_j} is the number of atoms in the R_j region and $N = \sum_{j=1}^{n} N_{R_j}$. The local pair correlation function of the

R_j region can be named $g(r)_{R_j}$:

$$g(r)_{R_j} = \frac{1}{4\pi r^2} \frac{1}{N_{R_j}\rho} \sum_{i\in R_j}\sum_{k\neq i} \langle \delta(r - |\vec{r}_k - \vec{r}_i|)\rangle, \quad \text{(A4)}$$

thus the pair correlation function is the superposition of many local pair correlation functions,

$$g(r) = \sum_{j=1}^{n} \frac{N_{R_j}}{N} g(r)_{R_j}. \quad \text{(A5)}$$

For an isotropic system, the structure factor $S(q)$ can be obtained by the Fourier transform of pair correlation function $g(r)$,

$$S(q) = 1 + \rho \int \frac{\sin(qr)}{qr}[g(r) - 1]4\pi r^2 dr. \quad \text{(A6)}$$

Bring Eq. (A5) into Eq. (A6) and change the order of summation $\sum \ldots$ and integration $\int \ldots$:

$$S(q) = 1 + \sum_{j=1}^{n} \frac{N_{R_j}}{N} \rho \int \frac{\sin(qr)}{qr}[g(r)_{R_j}-1]4\pi r^2 dr, \quad \text{(A7)}$$

$$S(q) = 1 + \sum_{j=1}^{n} \frac{N_{R_j}}{N}\left(1 + \rho \int \frac{\sin(qr)}{qr}[g(r)_{R_j} - 1]4\pi r^2 dr - 1\right), \quad \text{(A8)}$$

$$S(q) = 1 + \sum_{j=1}^{n} \frac{N_{R_j}}{N}\left(1 + \rho \int \frac{\sin(qr)}{qr}[g(r)_{R_j} - 1]4\pi r^2 dr\right) - \sum_{j=1}^{n} \frac{N_{R_j}}{N}, \quad \text{(A9)}$$

$$S(q) = \sum_{j=1}^{n} \frac{N_{R_j}}{N}\left(1 + \rho \int \frac{\sin(qr)}{qr}[g(r)_{R_j} - 1]4\pi r^2 dr\right), \quad \text{(A10)}$$

$$S(q) = \sum_{j=1}^{n} \frac{N_{R_j}}{N} S(q)_{R_j}. \quad \text{(A11)}$$

Thus the structure factor $S(q)$ can be rewritten as a weighted superposition of local structure factor $S(q)_{R_j}$ according to the proportion of atoms of the R_j region in the sample N_{R_j}/N.

2. Relationship between local SPLs (D_{q,R_j}) and total SPL (D_q) of metallic glasses

In the main text, we found that the reduced local SPL is proportional to the reduced ABM,

$$D_{q,R_j}/D_q \propto K_{R_j}/\bar{K}, \quad \text{(A12)}$$

where the $\bar{K}$ denotes the average bulk modulus. Furthermore, the above linear relation exhibits a crossover at point (1.0,1.0) in Fig. 5(b). Hence, we can describe Eq. (A12) by a linear function as Eq. (A13),

$$y = k(x - 1) + 1, \quad \text{(A13)}$$

where $y = D_{q,R_j}/D_q$ and $x = K_{R_j}/\bar{K}$. Bring y into Eq. (A13), then

$$D_{q,R_j} = k(x - 1)D_q + D_q. \quad \text{(A14)}$$

Similar to Eq. (A11), we calculate the weighted sum of local SPLs:

$$\sum_{j=1}^{n} \frac{N_{R_j}}{N} D_{q,R_j} = kD_q \sum_{j=1}^{n} \frac{N_{R_j}}{N}(x - 1) + \sum_{j=1}^{n} \frac{N_{R_j}}{N}D_q$$

$$= kD_q\left[\sum_{j=1}^{n} \frac{N_{R_j}}{N}x - \sum_{j=1}^{n} \frac{N_{R_j}}{N}\right] + D_q\sum_{j=1}^{n} \frac{N_{R_j}}{N}.$$

Since $\sum_{j=1}^{n} \frac{N_{R_j}}{N} = 1$, $x = \frac{K_{R_j}}{\bar{K}}$ (K_{R_j} indicates the numerical average of the ABM in the R_j region),

$$\sum_{j=1}^{n} \frac{N_{R_j}}{N} D_{q,R_j} = kD_q\left[\sum_{j=1}^{n} \frac{N_{R_j}}{N}\frac{K_{R_j}}{\bar{K}} - 1\right] + D_q$$

$$= kD_q\left[\frac{1}{\bar{K}}\sum_{j=1}^{n} \frac{N_{R_j}}{N}K_{R_j} - 1\right] + D_q$$

$$= kD_q\left[\frac{\tilde{K}}{\bar{K}} - 1\right] + D_q, \quad \text{(A15)}$$

where $\tilde{K} = \sum_{j=1}^{n} \frac{N_{R_j}}{N}K_{R_j}$ represents the numerical average of the ABM that is equal to the average bulk modulus, approximately $\tilde{K} \approx \bar{K}$,

$$\sum_{j=1}^{n} \frac{N_{R_j}}{N}D_{q,R_j} \approx D_q. \quad \text{(A16)}$$

Moreover, we have obtained the equivalence of SPLs in both real space and reciprocal space, i.e., $D_{r,R_j} = D_{q,R_j}$ and $D_r = D_q$,

$$\sum_{j=1}^{n} \frac{N_{R_j}}{N}D_{r,R_j} \approx D_r. \quad \text{(A17)}$$

Finally, we found that the weighted sum of local SPLs equals the SPL of samples in both real and reciprocal spaces.

[1] W. H. Wang, Prog. Mater. Sci. **57**, 487 (2012).

[2] Y. Q. Cheng and E. Ma, Prog. Mater. Sci. **56**, 379 (2011).

[3] T. C. Hufnagel, C. A. Schuh, and M. L. Falk, Acta Mater. **109**, 375 (2016).

[4] H. W. Sheng, W. K. Luo, F. M. Alamgir, J. M. Bai, and E. Ma, Nature (London) **439**, 419 (2006).

[5] D. B. Miracle, Nat. Mater. **3**, 697 (2004).

[6] A. Hirata, P. F. Guan, T. Fujita, Y. Hirotsu, A. Inoue, A. R. Yavari, T. Sakurai, and M. W. Chen, Nat. Mater. **10**, 28 (2011).

[7] J. D. Bernal and J. L. Finney, Discuss. Faraday Soc. **43**, 62 (1967).

[8] D. Z. Chen, C. Y. Shi, Q. An, Q. Zeng, W. L. Mao, W. A. Goddard, and J. R. Greer, Science **349**, 1306 (2015).

[9] D. Ma, A. D. Stoica, and X. L. Wang, Nat. Mater. **8**, 30 (2009).

[10] Q. Zeng, Y. Lin, Y. Liu, Z. Zeng, C. Y. Shi, B. Zhang, H. Lou, S. V. Sinogeikin, Y. Kono, and C. Kenney-Benson, Proc. Natl. Acad. Sci. USA **113**, 1714 (2016).

[11] J. Ding, M. Asta, and R. O. Ritchie, Proc. Natl. Acad. Sci. USA **114**, 8458 (2017).

[12] A. K. Gangopadhyay, M. E. Blodgett, M. L. Johnson, A. J. Vogt, N. A. Mauro, and K. F. Kelton, Appl. Phys. Lett. **104**, 191907 (2014).

[13] R. Li, L. Wang, L. Li, T. Yu, H. Zhao, K. W. Chapman, M. L. Rivers, P. J. Chupas, H.-k. Mao, and H. Liu, Phys. Rev. B **95**, 224204 (2017).

[14] H. Zhang, K. Qiao, and Y. Han, Nat. Commun. **11**, 2005 (2020).

[15] C. Xia, J. Li, B. Kou, Y. Cao, Z. Li, X. Xiao, Y. Fu, T. Xiao, L. Hong, J. Zhang *et al.*, Phys. Rev. Lett. **118**, 238002 (2017).

[16] M. Wu, J. Cheng, J. S. Tse, Y. Pan, and L. Zhang, Acta Mater. **141**, 75 (2017).

[17] J. Feng, P. Chen, and M. Li, Phys. Rev. B **98**, 024201 (2018).

[18] A. C. Wright, J. Non-Cryst. Solids **179**, 84 (1994).

[19] P. H. Gaskell and D. J. Wallis, Phys. Rev. Lett. **76**, 66 (1996).

[20] S. R. Elliott, Phys. Rev. Lett. **67**, 711 (1991).

[21] R. Shi and H. Tanaka, Sci. Adv. **5**, eaav3194 (2019).

[22] A. Zeidler and P. S. Salmon, Phys. Rev. B **93**, 214204 (2016).

[23] L. Li, L. Wang, R. Li, H. Zhao, D. Qu, K. W. Chapman, P. J. Chupas, and H. Liu, Phys. Rev. B **94**, 184201 (2016).

[24] S. Plimpton, J. Comput. Phys. **117**, 1 (1995).

[25] L. Zhong, J. Wang, H. Sheng, Z. Zhang, and S. X. Mao, Nature (London) **512**, 177 (2014).

[26] M. I. Mendelev, M. J. Kramer, R. T. Ott, D. J. Sordelet, D. Yagodin, and P. Popel, Philos. Mag. **89**, 967 (2009).

[27] Y. Q. Cheng, E. Ma, and H. W. Sheng, Phys. Rev. Lett. **102**, 245501 (2009).

[28] W. G. Hoover, Phys. Rev. A **31**, 1695 (1985).

[29] M. Parrinello and A. Rahman, J. Appl. Phys. **52**, 7182 (1981).

[30] H. Mizuno, S. Mossa, and J. L. Barrat, Phys. Rev. E **87**, 042306 (2013).

[31] See Supplemental Material at http://link.aps.org/supplemental/10.1103/PhysRevB.107.174207 for supplemental figures that describe the detailed evolution of pair correlation functions and structure factors (Fig. S1), the fitting of SPLs for Cu, $Cu_{50}Zr_{50}$, and $Zr_{50}Cu_{40}Al_{10}$ MGs (Fig. S2), average local strain under different cutoff distances (Fig. S3), and the ratio of local SPLs of real space to local SPLs of reciprocal space (Fig. S4).

[32] G. S. Cargill, Solid State Phys. **30**, 227 (1975).

[33] Y. Suzuki, J. Haimovich, and T. Egami, Phys. Rev. B **35**, 2162 (1987).

[34] D. Ma, A. D. Stoica, X. L. Wang, Z. P. Lu, B. Clausen, and D. W. Brown, Phys. Rev. Lett. **108**, 085501 (2012).

[35] H. F. Poulsen, J. A. Wert, J. Neuefeind, V. Honkimäki, and M. Daymond, Nat. Mater. **4**, 33 (2004).

[36] H. Wagner, D. Bedorf, S. Kuchemann, M. Schwabe, B. Zhang, W. Arnold, and K. Samwer, Nat. Mater. **10**, 439 (2011).

[37] B. A. Sun, Y. C. Hu, D. P. Wang, Z. G. Zhu, P. Wen, W. H. Wang, C. T. Liu, and Y. Yang, Acta Mater. **121**, 266 (2016).

[38] H. Mizuno, L. E. Silbert, and M. Sperl, Phys. Rev. Lett. **116**, 068302 (2016).

[39] Y. C. Hu, P. F. Guan, M. Z. Li, C. T. Liu, Y. Yang, H. Y. Bai, and W. H. Wang, Phys. Rev. B **93**, 214202 (2016).

[40] X. Wei, B. Xu, and P. Guan, J. Non-Cryst. Solids **578**, 121345 (2022).

[41] Y. H. Liu, D. Wang, K. Nakajima, W. Zhang, A. Hirata, T. Nishi, A. Inoue, and M. W. Chen, Phys. Rev. Lett. **106**, 125504 (2011).

[42] M. Gao and J. H. Perepezko, Nano Lett. **20**, 7558 (2020).

[43] S. S. Sørensen, C. A. Biscio, M. Bauchy, L. Fajstrup, and M. M. Smedskjaer, Sci. Adv. **6**, eabc2320 (2020).

[44] F. Zhu, A. Hirata, P. Liu, S. Song, Y. Tian, J. Han, T. Fujita, and M. Chen, Phys. Rev. Lett. **119**, 215501 (2017).

[45] K. Binder and W. Kob, *Glassy Materials and Disordered Solids: An Introduction to their Statistical Mechanics* (World Scientific, Singapore, 2011).